PHYSICS

Giant gate-tunable bandgap renormalization and excitonic effects in a 2D semiconductor

Zhizhan Qiu[1,2]*, Maxim Trushin[3]*, Hanyan Fang[1]*, Ivan Verzhbitskiy[3,4], Shiyuan Gao[5], Evan Laksono[3,4], Ming Yang[6], Pin Lyu[1], Jing Li[1], Jie Su[1,3], Mykola Telychko[1,3], Kenji Watanabe[7], Takashi Taniguchi[7], Jishan Wu[1], A. H. Castro Neto[3,4], Li Yang[5], Goki Eda[1,3,4], Shaffique Adam[3,4,8], Jiong Lu[1,3]†

Understanding the remarkable excitonic effects and controlling the exciton binding energies in two-dimensional (2D) semiconductors are crucial in unlocking their full potential for use in future photonic and optoelectronic devices. Here, we demonstrate large excitonic effects and gate-tunable exciton binding energies in single-layer rhenium diselenide ($ReSe_2$) on a back-gated graphene device. We used scanning tunneling spectroscopy and differential reflectance spectroscopy to measure the quasiparticle electronic and optical bandgap of single-layer $ReSe_2$, respectively, yielding a large exciton binding energy of 520 meV. Further, we achieved continuous tuning of the electronic bandgap and exciton binding energy of monolayer $ReSe_2$ by hundreds of milli–electron volts through electrostatic gating, attributed to tunable Coulomb interactions arising from the gate-controlled free carriers in graphene. Our findings open a new avenue for controlling the bandgap renormalization and exciton binding energies in 2D semiconductors for a wide range of technological applications.

INTRODUCTION

Atomically thin two-dimensional (2D) semiconductors usually exhibit large bandgap renormalization and extraordinary excitonic effects due to quantum confinement and reduced dielectric screening (*1*–*4*). As a result, light-matter interactions in these systems are primarily governed by the enhanced excitonic effects, which have been exploited to develop exciton-based devices operated at room temperature (RT) (*5*). Future progress in this area hinges on the ability to control the excitonic effects of 2D semiconductors by precisely tuning their exciton binding energies (E_b). This is crucial for realizing the full potential of 2D semiconductors in photonic and optoelectronic applications.

One unique aspect of 2D semiconductors is their unprecedented tunability in both their electronic and optical properties, due to high susceptibility to the doping and environmental screening (*1*, *6*–*12*). It has been theoretically predicted and experimentally demonstrated that Coulomb interactions in 2D semiconductors can be engineered to tune their quasiparticle (QP) bandgap (E_g) and E_b using different methods such as chemical doping (*6*), electrostatically gating (*7*), and engineering environmental screening (*1*, *8*, *9*, *11*, *12*). Among all the methods reported, electrostatic gating offers additional advantages including continuous tunability and excellent compatibility for integration in modern device technologies. Recent studies involving the use of optical measurements demonstrated that gate-controlled excitonic effects can be achieved in monolayer transition metal dichalcogenides (TMDs) (*7*). However, an overlap of the band-edge absorption step with strong excitonic resonances generally makes it challenging to accurately determine E_g of 2D semiconductors from their optical absorption spectrum (*13*).

To probe E_b of 2D semiconductors directly, one can use scanning tunneling spectroscopy (STS) and optical spectroscopy (e.g., differential reflectance or photoluminescence spectroscopy) to measure E_g and optical bandgap (E_{opt}), respectively (*1*, *14*). Here, we used this approach to demonstrate the gate-tunable E_g and excitonic effects in monolayer $ReSe_2$ on a back-gated graphene field-effect transistor (FET) device, as sketched in Fig. 1A. We observed a large E_b of 520 meV for monolayer $ReSe_2$ at zero gate voltage (V_g = 0 V). Moreover, we show that E_b of monolayer $ReSe_2$ can be continuously tuned from 460 to 680 meV by electrostatic gating, which can be mainly attributed to screening from gate-controlled free carriers in graphene. This is distinct from the previous study of gate-tunable E_b in 2D semiconductors wherein the semiconductors' own free carriers play a major role (*7*). These 2D semiconductor/graphene heterostructures have been widely used in the fabrication of transistors (*15*–*17*), photo detectors (*18*), and energy-harvesting devices (*19*). The ability to precisely tune the bandgap and excitonic effects of 2D semiconductors on graphene provides a new route for the optimization of the interfacial charge transport or light-harvesting efficiency. Therefore, we expect that our findings would have a profound impact in the field of novel electronic and optoelectronic devices based on artificially engineered van der Waals heterostructures.

RESULTS

Topographic imaging of monolayer $ReSe_2$ on graphene

Unlike hexagonal TMDs, monolayer $ReSe_2$ adopts a distorted 1*T* structure with triclinic symmetry (Fig. 1B), wherein four Re atoms slip off from their regular octahedral sites due to the charge decoupling from their d^3 electrons. This results in the formation of a 1D chain-like structure consisting of interconnected diamond-shaped Re_4 units along the *a* direction as shown in Fig. 1B (*20*, *21*). Because of this, monolayer $ReSe_2$ exhibits unique in-plane anisotropic electronic and

[1]Department of Chemistry, National University of Singapore, 3 Science Drive 3, Singapore 117543, Singapore. [2]NUS Graduate School for Integrative Sciences and Engineering, National University of Singapore, 28 Medical Drive, Singapore 117456, Singapore. [3]Centre for Advanced 2D Materials (CA2DM), National University of Singapore, 6 Science Drive 2, Singapore 117546, Singapore. [4]Department of Physics, National University of Singapore, 2 Science Drive 3, Singapore 117551, Singapore. [5]Department of Physics, Washington University in St. Louis, St. Louis, MO 63130, USA. [6]Institute of Materials Research and Engineering, Agency for Science, Technology and Research (A*STAR), 2 Fusionopolis Way, Singapore 138634, Singapore. [7]National Institute of Materials Science, 1-1 Namiki, Tsukuba 305-0044, Japan. [8]Yale-NUS College, 16 College Avenue West, Singapore 138527, Singapore.
*These authors contributed equally to this work.
†Corresponding author. Email: chmluj@nus.edu.sg

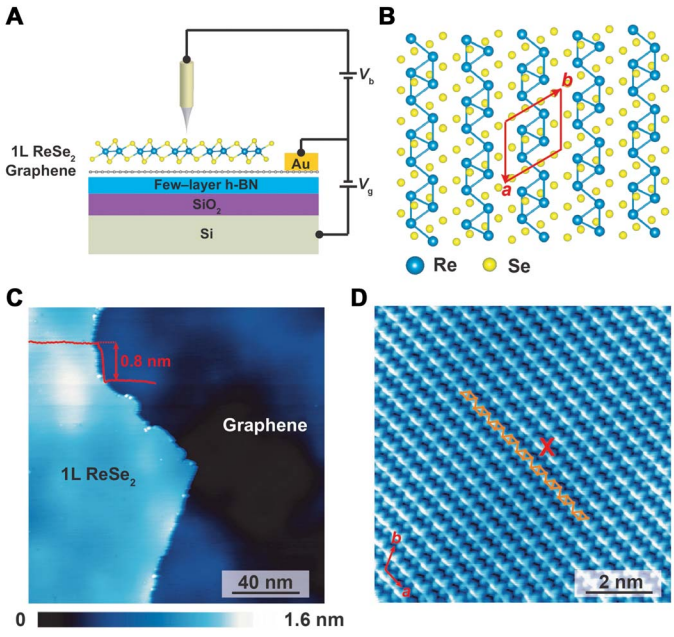

Fig. 1. A monolayer $ReSe_2$ on a back-gated G/h-BN device. (**A**) Schematic illustration of a back-gated $ReSe_2$/graphene/h-BN device. (**B**) Top view of the atomic structure of monolayer $ReSe_2$. The two lattice vectors (*a* and *b*) are outlined by red lines. The lattice constants are $a = 6.6$ Å and $b = 6.7$ Å. The angle between *a* and *b* is 118.9°. (**C**) A representative STM image of a monolayer $ReSe_2$ flake on graphene/h-BN. Inset shows the STM line profile along the step edge. (**D**) Atomically resolved STM image of monolayer $ReSe_2$. The STM image reveals the unique 1D chains consisting of diamond-shaped Re_4 units along *a* direction (highlighted by orange line). The cross (X) marks the position where the differential conductance (d*I*/d*V*) spectra were taken.

optical properties, making it particularly attractive for near-infrared polarization-sensitive optoelectronic applications (*22*).

To probe the carrier-dependent excitonic effects, we transferred a monolayer $ReSe_2$ flake onto a clean back-gated graphene FET device consisting of a chemical vapor deposition–grown graphene monolayer placed on a hexagonal boron nitride (h-BN) flake that rests on a SiO_2 layer above a doped Si wafer (Fig. 1A). In contrast to the SiO_2 substrate, the atomic flatness of the underlying h-BN markedly reduces the surface roughness and charge inhomogeneity in graphene (*6*, *23*, *24*). The use of graphene not only enables the direct scanning tunneling microscopy (STM) measurement of the gated single-layer $ReSe_2$ but also improves the electrical contact to monolayer $ReSe_2$ (*25*–*27*).

Figure 1C shows a representative STM image of a monolayer $ReSe_2$ flake placed on the monolayer graphene/h-BN substrate. The STM height profile across the step edge of the $ReSe_2$ flake reveals an apparent height of ~0.8 Å, suggesting monolayer thickness (fig. S1). Further, the atomically resolved STM image (Fig. 1D) reveals a diamond chain-like structure as expected for monolayer $ReSe_2$ with a distorted 1*T* atomic structure (*21*). The lattice constants of $ReSe_2$ along the *a* and *b* directions (as marked in Fig. 1, B and D) are determined to be 6.6 ± 0.1 Å and 6.7 ± 0.1 Å, respectively, which are in good agreement with the previous study (*20*). It is also expected that moiré patterns would arise when the graphene was overlaid with the monolayer $ReSe_2$ at different twist angles. Several representative moiré patterns have been successfully captured in our STM images of different spatial regions of different samples (Fig. 2, A to C). Distinct from most twisted 2D heterostructures such as graphene on h-BN (*28*), the moiré patterns of $ReSe_2$/graphene exhibit two different periods along two crystallographic orientations (as marked by L_1 and L_2 in Fig. 2, A to F). This is due to the stacking of monolayer $ReSe_2$ with triclinic lattice symmetry on graphene with a honeycomb lattice. The unique moiré patterns observed here can be well reproduced (Fig. 2, D to F) using the geometrical analysis of twist angle–dependent moiré patterns of $ReSe_2$/graphene heterostructures (refer to section S2 for more details).

Electronic structure of monolayer $ReSe_2$

We then probed the local electronic properties of $ReSe_2$ using STS. We note that differential conductance (d*I*/d*V*) spectra acquired in several moiré regions exhibit similar features (refer to section S3 for more details). Figure 3A shows a representative d*I*/d*V* spectrum acquired over monolayer $ReSe_2$ (marked by a cross in Fig. 1D) at $V_g = 0$ V together with the local density of states (LDOS) calculated by density functional theory (refer to section S5 for more details). A wide bandgap and several prominent resonant peaks located close to both the conduction band (CB) and valence band (VB) edges have been captured in the d*I*/d*V* spectrum taken on the clean surface region (solid blue line in Fig. 3A). These features can be well reproduced in the calculated LDOS of a free-standing monolayer $ReSe_2$ (dashed red line in Fig. 3A and refer to section S5 for more details). A close examination of the calculated band structure of monolayer $ReSe_2$ allows us to identify that the origin of the prominent resonant peaks at the CB side (C_1) is attributed to the dispersionless electronic bands as indicated in fig. S5.

We identify the band edges of each d*I*/d*V* spectrum using the method previously reported (*1*). The VB maximum (VBM) and the CB minimum (CBM) are found to be located at −1.27 ± 0.01 eV and 0.72 ± 0.01 eV, respectively, which yields E_g of 1.99 ± 0.02 eV for monolayer $ReSe_2$. In addition, we observe the Fermi level (E_F) to be closer to the CBM than the VBM, indicating a low n-doping of $ReSe_2$, which is presumably due to the presence of donor-like defects with shallow mid-gap states (fig. S4A).

Gate-tunable QP bandgap renormalization

One unique aspect of this study is that we can probe the QP band structures as a function of gate voltage. Figure 3C shows the gate-dependent d*I*/d*V* spectra taken at the same position over monolayer $ReSe_2$. We observed that a gate-dependent rigid shift of the CBM and C_1 toward E_F when V_g is changed from −63 to +45 V (Fig. 3, B and C). Unexpectedly, the VBM remains nearly constant at different gate voltages as shown in Fig. 3 (B and C). The distinct shift of the CBM and VBM with the increase in the applied gate voltage therefore indicates a monotonic reduction of E_g. The QP bandgap of monolayer $ReSe_2$ is determined to be 2.15 ± 0.01 eV at $V_g = -63$ V and 1.93 ± 0.02 eV at $V_g = 45$ V, respectively.

Probing the optical bandgap of monolayer $ReSe_2$

We performed the differential reflectance spectroscopic measurement of monolayer $ReSe_2$/graphene/h-BN at 5 K to probe its optical bandgap. Differential reflectance spectra of the sample after the background subtraction are shown in Fig. 3D (refer to fig. S6A for more details). At $V_g = 0$ V, E_{opt} of monolayer $ReSe_2$ is determined to be 1.47 ± 0.01 eV at 5 K based on the peak position of differential reflectance spectrum (Fig. 3D), consistent with previous results (*22*). To probe the electrostatic gating effect on E_{opt}, we monitored the evolution of the peak position of the hybrid $ReSe_2$/graphene device as a function of gate voltage.

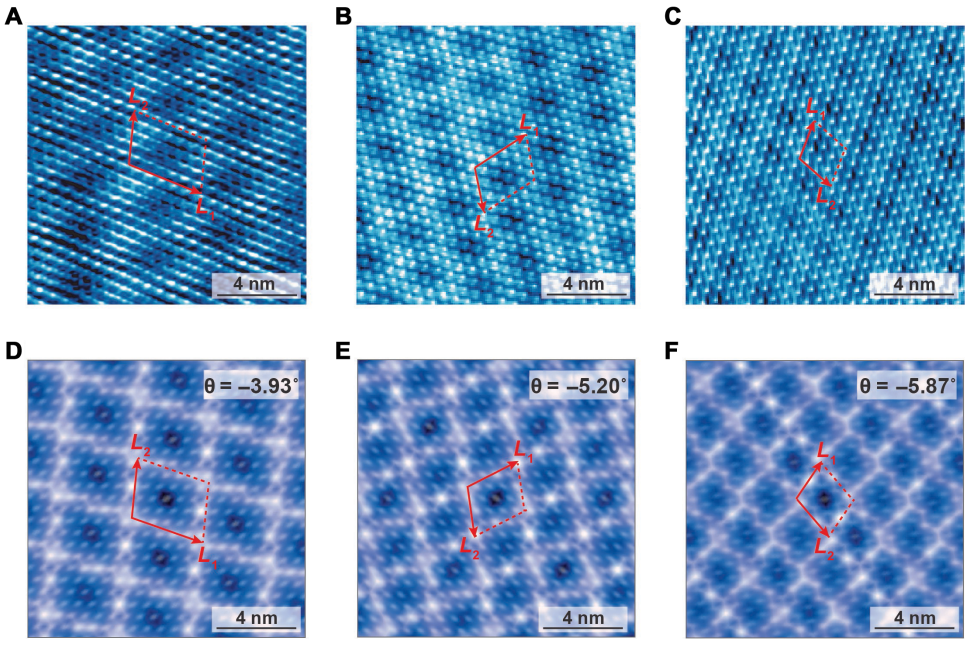

Fig. 2. STM images of moiré pattern in monolayer $ReSe_2$/graphene. (**A** to **C**) Representative moiré patterns observed in the experiment. (**D** to **F**) Calculated moiré patterns obtained from the geometrical analysis. θ is the stacking angle between $ReSe_2$ and graphene.

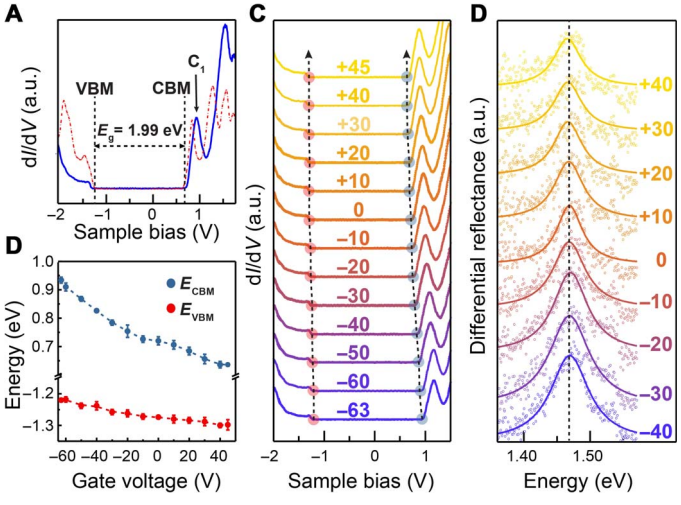

Fig. 3. Gate-dependent d*I*/d*V* and differential reflectance spectra of a monolayer $ReSe_2$ on graphene. (**A**) d*I*/d*V* spectrum of monolayer $ReSe_2$ (blue line) at V_g = 0 V together with the calculated LDOS (dashed red line). (**B**) Energy position of VB maximum (VBM; red points) and CB minimum (CBM; dark blue points) as a function of the gate voltage. (**C**) Gate-dependent d*I*/d*V* spectra of the monolayer $ReSe_2$ on graphene/h-BN measured at 4.5 K. As-applied gate voltage is indicated above each STS curve. The VBM and CBM were indicated by light red and light blue points, respectively. (**D**) Gate-dependent differential reflectance spectra of the monolayer $ReSe_2$ on graphene/h-BN measured at 5 K. The corresponding gate voltage is indicated on the side of each differential reflectance spectrum. Note: The original differential reflectance spectra after background subtraction (circles); fitted curves using the Lorentzian function (solid lines). a.u., arbitrary units.

We found that E_{opt} remains nearly constant at all the gate voltages as opposed to the monotonic reduction of E_g (Fig. 3, C and D). It reflects that the renormalization of E_g is nearly fully offset by the change of E_b, in agreement with Koopmans' theorem adapted for semiconductors and previous experimental studies (*9*, *29*, *30*). To further verify this, we performed photoluminescence measurement of monolayer $ReSe_2$/graphene/h-BN at different gate voltages at RT. The gate-dependent photoluminescence spectra acquired at RT also reveal a nearly constant E_{opt} of monolayer $ReSe_2$ (fig. S6B).

Gate-tunable exciton binding energy

The exciton binding energy is directly determined from the equation ($E_b = E_g - E_{opt}$). As shown in Fig. 4A, a large gate-tunable bandgap renormalization of $ReSe_2$ can be achieved in our hybrid device, whereby E_b can be precisely tuned over a wide energy range from 680 ± 20 meV to 460 ± 20 meV when V_g increases from −63 to +45 V. The pertinent question to be addressed in this work is the physical origins of the gate-tunable QP bandgap renormalization and exciton binding energy in monolayer $ReSe_2$. We are able to exclude the contribution from the out-of-plane field-induced polarization of CBM and VBM wave functions (namely, Stark effects). The vertical field induced polarization of electrons and holes in monolayer TMDs is negligible due to their extreme confinement in the in-plane direction (*7*). In addition, the screening by graphene substrate substantially reduces the vertical electric field effect for monolayer $ReSe_2$.

On the other hand, free carriers in both $ReSe_2$ and adjacent graphene can, in principle, contribute to the renormalization of E_g and tunable E_b in single-layer $ReSe_2$. It has been predicted that E_g of a free-standing 2D semiconductor can be substantially reduced because of the presence of free carriers (*31*, *32*). Further, the dominant contribution to the QP bandgap renormalization in these systems is predicted to arise from the Coulomb-hole self-energy and screened-exchange self-energy (*31*). However, a detailed analysis of the experimental data reveals that the renormalization of E_g and tunable E_b is not likely to arise from the presence of free carriers in $ReSe_2$. First, the set of gate-dependent d*I*/d*V* spectra shows that E_F never crosses the band edge of $ReSe_2$ (Fig. 3C), suggesting the absence of free carriers residing in the band edge states. We also considered the potential free carriers contributed from point

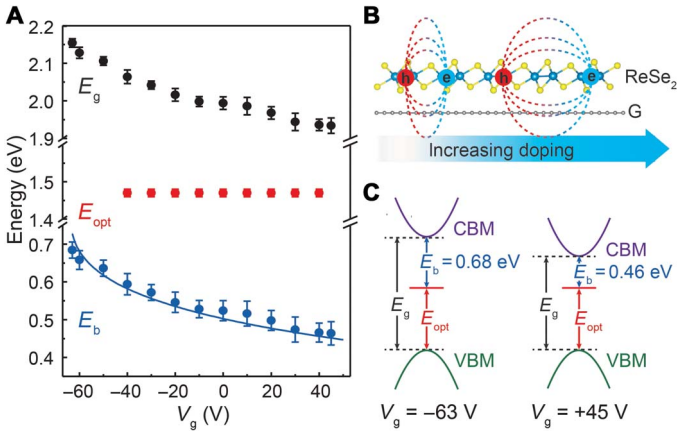

Fig. 4. Gate-tunable bandgap renormalization and exciton binding energy of monolayer $ReSe_2$ on graphene. (**A**) A plot of QP bandgap E_g (black points), optical bandgap E_{opt} (red points), and exciton binding energy E_b (blue points) as a function of gate voltage. Note: The E_{opt} = 1.47 ± 0.01 eV remains constant when the gate voltage increases from −40 to 40 V. Note: The same E_{opt} is used for the calculation of E_b at the gate voltage of −63, −60, −50, and +45 V. The solid blue line refers to the theoretically predicted E_b as a function of the gate voltage (refer to section S8 for more details). (**B**) Illustration of the screening of electron-hole interactions in monolayer $ReSe_2$ by the gate-controlled free carriers in graphene. (**C**) Schematic illustration of gate-tunable E_g and E_b of monolayer $ReSe_2$ at the gate voltage of −63 and +45 V, respectively.

defects with shallow mid-gap states in $ReSe_2$ (refer to section S4 for more details), although our gate-dependent dI/dV spectra of monolayer $ReSe_2$ are taken in the region free of defects. However, our STM imaging and spectroscopy measurements reveal that these defects with a low density of ~3.9 (± 1.5) × 10^{11} cm^{-2} are electronically isolated from each other (fig. S4). Therefore, the carriers localized around these defects are not likely to play a significant role in the renormalization of E_g.

These observations suggest that bandgap renormalization and tunable E_b of monolayer $ReSe_2$ are the result of the gate-induced free carriers in graphene. To further examine our hypothesis, we performed the gate-dependent STS measurement of a new device consisting of monolayer graphene stacked on top of a monolayer $ReSe_2$ on SiO_2/Si substrate. By reversing the stacking order (graphene/$ReSe_2$), we are able to measure gate-dependent Dirac point (E_D) of graphene and E_g of monolayer $ReSe_2$ simultaneously (refer to section S7 for more details). The results also show a gate-tunable bandgap renormalization of monolayer $ReSe_2$ (fig. S7F). Moreover, it is observed that E_g of $ReSe_2$ reaches the maximum close to the charge neutrality point of graphene and reduces monotonically upon increase in either n-doping or p-doping of graphene (fig. S7F). Thus, a simultaneous measurement of both E_g of $ReSe_2$ and doping in graphene demonstrates that the observed gate-tunable bandgap renormalization and excitonic effects in monolayer $ReSe_2$ are attributed to the screening from the gate-controlled free carriers in the adjacent graphene.

We then used a quasi-classical model based on the Thomas-Fermi screening theory (refer to section S8 for more details) to calculate E_b of monolayer $ReSe_2$ on graphene/h-BN as a function of the carrier density in graphene (n). The screening model comprises two components: the Thomas-Fermi screening radius due to the free electrons in graphene and an effective dielectric constant (ε_{eff} = 6.09) that accounts for the combined dielectric permittivity of h-BN and $ReSe_2$ (see section S8 for derivation). Our theoretical results show that a moderate doping (n about 8 × 10^{12} cm^{-2}) in graphene substantially reduces the exciton binding energy by hundreds of milli–electron volts, resulting in a monotonic decrease in E_b as the free-carrier concentration in graphene increases (fig. S8A).

To directly compare with experimental results, we need to convert the carrier density in graphene to the corresponding gate voltage (V_g). The carrier density in the $ReSe_2$/graphene hybrid system depends linearly on the gate voltage: $n = \alpha(V_g - V_0)$. Here, α is estimated to be around 7.1 × 10^{10} cm^{-2} V^{-1} using a standard capacitor model (consisting of ~285-nm SiO_2 and ~15-nm h-BN as dielectric materials) (*33*, *34*). Note that αV_0 is the initial doping of the system at V_g = 0 V. Since the density of defects with mid-gap states is extremely low (3.9 (± 1.5) × 10^{11} cm^{-2}) compared with the total gate-induced free-carrier density (Δn = 7.7 × 10^{12} cm^{-2}) and E_F is away from band edges of $ReSe_2$, this rationalizes that most of the gate-induced free carriers are injected into the underlying graphene. When V_0 is set as −64 V, we find the calculated E_b as a function of gate voltage agrees with the observed gate-dependent E_b (Fig. 4A). This suggests that the graphene underneath monolayer $ReSe_2$ is strongly n-doped at V_g = 0 V, in line with the charge transfer analysis discussed in section S9.

DISCUSSION

In summary, we have successfully tailored the QP bandgap and the exciton binding energy in a 2D semiconductor by controlling the doping in the underlying graphene using electrostatic gating. Our results show that screening from a graphene substrate has a profound impact on Coulomb interactions in adjacent 2D semiconductors and leads to broad tunability of the electronic bandgap and exciton binding energy. Our findings not only result in the unprecedented understanding of many-electron physics in hybrid 2D semiconductor/graphene systems but also pave the way toward controlling the excitonic effects and precisely tuning the exciton binding energies in 2D semiconductors for a wide range of technological applications.

MATERIALS AND METHODS

Sample preparation

We fabricated the graphene/h-BN sample based on the recipe reported previously (*35*). We then used the well-established dry transfer technique to place a monolayer $ReSe_2$ on top of graphene/h-BN sitting on SiO_2/Si substrate (*36*). The key steps for the sample treatment include the following: (i) The h-BN/SiO_2/Si substrate was annealed in the furnace at 500°C for 2 hours before the transfer of graphene. (ii) After the transfer of graphene, graphene/h-BN/SiO_2/Si sample was annealed in furnace with a flow of 100 sccm (standard cubic centimeters per minute) H_2 and 200 sccm Ar at 350°C for 5 hours. (iii) $ReSe_2$/graphene/h-BN was annealed at 300°C in the ultrahigh vacuum chamber for 12 hours.

STM and STS measurements

Our STM and STS measurements were conducted at 4.5 K in the Omicron LT-STM system with a base pressure lower than 10^{-10} mbar. The STM tip was calibrated spectroscopically against the surface state of Au(111) substrate. All the dI/dV spectra were measured through a standard lock-in technique with a modulated voltage of 5 to 10 mV and the frequency of 700 to 800 Hz.

Differential reflectance and photoluminescence measurements

The differential reflectance measurements and photoluminescence measurements were conducted at 5 K and at RT, respectively, using a

custom-built confocal spectrometer. For differential reflectance measurements, samples were illuminated by the white light from broadband source (hydrogen-halogen lamp) focused into the spot of ~2 μm. Reflectance spectra from monolayer $ReSe_2$ (R_{ReSe_2}) and substrate (R_{sub}) were collected in confocal geometry. Differential reflectance spectra (DR) are obtained by $DR = (R_{sub} - R_{ReSe_2})/R_{sub}$. For photoluminescence measurements, samples were excited with a 532-nm laser through the 100× objective lens (numerical aperture of 0.9) with a power below 0.5 mW.

SUPPLEMENTARY MATERIALS

Supplementary material for this article is available at http://advances.sciencemag.org/cgi/content/full/5/7/eaaw2347/DC1

Section S1. Atomic force microscopy measurement of monolayer $ReSe_2$
Section S2. Moiré pattern of single-layer $ReSe_2$ on graphene
Section S2.1. Moiré patterns for various twist angles
Section S2.2. A comparison between experimental and theoretical moiré patterns
Section S3. Gate-dependent d*I*/d*V* spectra of a different $ReSe_2$/graphene device
Section S4. Probe the defects in monolayer $ReSe_2$
Section S5. Band structure of monolayer $ReSe_2$
Section S6. Differential reflectance spectrum and gate-dependent photoluminescence spectra of monolayer $ReSe_2$
Section S7. Gate-dependent d*I*/d*V* spectra of graphene/monolayer $ReSe_2$
Section S8. Calculation of E_b in monolayer $ReSe_2$ as a function of the carrier density in graphene substrate
Section S9. Charge transfer at the interface of $ReSe_2$/graphene
Fig. S1. Identify the thickness of monolayer $ReSe_2$.
Fig. S2. Moiré lengths of $ReSe_2$/graphene as a function of twist angle.
Fig. S3. Gate-dependent d*I*/d*V* spectra of a different device.
Fig. S4. STM images and STS measurements of defects in $ReSe_2$.
Fig. S5. Band structure of monolayer $ReSe_2$ calculated using the first-principle density functional theory calculations with the Perdew-Burke-Ernzerhof exchange-correlation functional using the QUANTUM ESPRESSO code.
Fig. S6. Differential reflectance spectrum and gate-dependent photoluminescence spectra of monolayer $ReSe_2$ on graphene/h-BN.
Fig. S7. Gate-dependent d*I*/d*V* spectra of graphene/monolayer $ReSe_2$.
Fig. S8. Exciton binding energy (E_b) and Thomas-Fermi screening radius (r_s) as a function of electron concentration (n) in graphene.
Fig. S9. Charge transfer at $ReSe_2$/graphene interface.
Table S1. Geometrical properties of the moiré patterns of $ReSe_2$/graphene.
References (*37*–*46*)

REFERENCES AND NOTES

1. M. M. Ugeda, A. J. Bradley, S.-F. Shi, F. H. da Jornada, Y. Zhang, D. Y. Qiu, W. Ruan, S.-K. Mo, Z. Hussain, Z.-X. Shen, F. Wang, S. G. Louie, M. F. Crommie, Giant bandgap renormalization and excitonic effects in a monolayer transition metal dichalcogenide semiconductor. *Nat. Mater.* **13**, 1091–1095 (2014).
2. H.-P. Komsa, A. V. Krasheninnikov, Effects of confinement and environment on the electronic structure and exciton binding energy of MoS_2 from first principles. *Phys. Rev. B* **86**, 241201 (2012).
3. K. He, N. Kumar, L. Zhao, Z. Wang, K. F. Mak, H. Zhao, J. Shan, Tightly bound excitons in monolayer WSe_2. *Phys. Rev. Lett.* **113**, 026803 (2014).
4. D. Y. Qiu, F. H. da Jornada, S. G. Louie, Optical spectrum of MoS_2: Many-body effects and diversity of exciton states. *Phys. Rev. Lett.* **111**, 216805 (2013).
5. D. Unuchek, A. Ciarrocchi, A. Avsar, K. Watanabe, T. Taniguchi, A. Kis, Room-temperature electrical control of exciton flux in a van der Waals heterostructure. *Nature* **560**, 340–344 (2018).
6. J. Katoch, S. Ulstrup, R. J. Koch, S. Moser, K. M. McCreary, S. Singh, J. Xu, B. T. Jonker, R. K. Kawakami, A. Bostwick, E. Rotenberg, C. Jozwiak, Giant spin-splitting and gap renormalization driven by trions in single-layer WS_2/h-BN heterostructures. *Nat. Phys.* **14**, 355–359 (2018).
7. A. Chernikov, A. M. van der Zande, H. M. Hill, A. F. Rigosi, A. Velauthapillai, J. Hone, T. F. Heinz, Electrical tuning of exciton binding energies in monolayer WS_2. *Phys. Rev. Lett.* **115**, 126802 (2015).
8. R. Kumar, I. Verzhbitskiy, F. Giustiniano, T. P. H. Sidiropoulos, R. F. Oulton, G. Eda, Interlayer screening effects in WS_2/WSe_2 van der Waals hetero-bilayer. *2D Mater.* **5**, 041003 (2018).
9. A. Raja, A. Chaves, J. Yu, G. Arefe, H. M. Hill, A. F. Rigosi, T. C. Berkelbach, P. Nagler, C. Schüller, T. Korn, C. Nuckolls, J. Hone, L. E. Brus, T. F. Heinz, D. R. Reichman, A. Chernikov, Coulomb engineering of the bandgap and excitons in two-dimensional materials. *Nat. Commun.* **8**, 15251 (2017).
10. D. Y. Qiu, F. H. da Jornada, S. G. Louie, Environmental screening effects in 2D materials: Renormalization of the bandgap, electronic structure, and optical spectra of few-layer black phosphorus. *Nano Lett.* **17**, 4706–4712 (2017).
11. S. Park, N. Mutz, T. Schultz, S. Blumstengel, A. Han, A. Aljarb, L.-J. Li, E. J. List-Kratochvil, P. Amsalem, N. Koch, Direct determination of monolayer MoS_2 and WSe_2 exciton binding energies on insulating and metallic substrates. *2D Mater.* **5**, 025003 (2018).
12. Q. Zhang, Y. Chen, C. Zhang, C.-R. Pan, M.-Y. Chou, C. Zeng, C.-K. Shih, Bandgap renormalization and work function tuning in $MoSe_2$/hBN/Ru (0001) heterostructures. *Nat. Commun.* **7**, 13843 (2016).
13. G. Wang, A. Chernikov, M. M. Glazov, T. F. Heinz, X. Marie, T. Amand, B. Urbaszek, *Colloquium*: Excitons in atomically thin transition metal dichalcogenides. *Rev. Mod. Phys.* **90**, 021001 (2018).
14. C. Zhang, A. Johnson, C.-L. Hsu, L.-J. Li, C.-K. Shih, Direct imaging of band profile in single layer MoS_2 on graphite: Quasiparticle energy gap, metallic edge states, and edge band bending. *Nano Lett.* **14**, 2443–2447 (2014).
15. T. Georgiou, R. Jalil, B. D. Belle, L. Britnell, R. V. Gorbachev, S. V. Morozov, Y.-J. Kim, A. Gholinia, S. J. Haigh, O. Makarovsky, L. Eaves, L. A. Ponomarenko, A. K. Geim, K. S. Novoselov, A. Mishchenko, Vertical field-effect transistor based on graphene–WS_2 heterostructures for flexible and transparent electronics. *Nat. Nanotechnol.* **8**, 100–103 (2013).
16. S. Bertolazzi, D. Krasnozhon, A. Kis, Nonvolatile memory cells based on MoS_2/graphene heterostructures. *ACS Nano* **7**, 3246–3252 (2013).
17. W. J. Yu, Z. Li, H. Zhou, Y. Chen, Y. Wang, Y. Huang, X. Duan, Vertically stacked multi-heterostructures of layered materials for logic transistors and complementary inverters. *Nat. Mater.* **12**, 246–252 (2013).
18. K. Roy, M. Padmanabhan, S. Goswami, T. P. Sai, G. Ramalingam, S. Raghavan, A. Ghosh, Graphene–MoS_2 hybrid structures for multifunctional photoresponsive memory devices. *Nat. Nanotechnol.* **8**, 826–830 (2013).
19. L. Britnell, R. Ribeiro, A. Eckmann, R. Jalil, B. Belle, A. Mishchenko, Y.-J. Kim, R. V. Gorbachev, T. Georgiou, S. V. Morozov, A. N. Grigorenko, A. K. Geim, C. Casiraghi, A. H. Castro Neto, K. S. Novoselov, Strong light-matter interactions in heterostructures of atomically thin films. *Science* **340**, 1311–1314 (2013).
20. B. Jariwala, A. Thamizhavel, A. Bhattacharya, $ReSe_2$: A reassessment of crystal structure and thermal analysis. *J. Phys. D Appl. Phys.* **50**, 044001 (2016).
21. M. Hong, X. Zhou, N. Gao, S. Jiang, C. Xie, L. Zhao, Y. Gao, Z. Zhang, P. Yang, Y. Shi, Q. Zhang, Z. Liu, J. Zhao, Y. Zhang, Identifying the non-identical outermost selenium atoms and invariable band gaps across the grain boundary of anisotropic rhenium diselenide. *ACS Nano* **12**, 10095–10103 (2018).
22. A. Arora, J. Noky, M. Drüppel, B. Jariwala, T. Deilmann, R. Schneider, R. Schmidt, O. Del Pozo-Zamudio, T. Stiehm, A. Bhattacharya, Highly anisotropic in-plane excitons in atomically thin and bulklike 1T′-$ReSe_2$. *Nano Lett.* **17**, 3202–3207 (2017).
23. A. K. Geim, I. V. Grigorieva, Van der Waals heterostructures. *Nature* **499**, 419–425 (2013).
24. C. R. Dean, A. F. Young, I. Meric, C. Lee, L. Wang, S. Sorgenfrei, K. Watanabe, T. Taniguchi, P. Kim, K. L. Shepard, J. Hone, Boron nitride substrates for high-quality graphene electronics. *Nat. Nanotechnol.* **5**, 722–726 (2010).
25. A. Allain, J. Kang, K. Banerjee, A. Kis, Electrical contacts to two-dimensional semiconductors. *Nat. Mater.* **14**, 1195–1205 (2015).
26. W. S. Leong, X. Luo, Y. Li, K. H. Khoo, S. Y. Quek, J. T. L. Thong, Low resistance metal contacts to MoS_2 devices with nickel-etched-graphene electrodes. *ACS Nano* **9**, 869–877 (2014).
27. T. Roy, M. Tosun, J. S. Kang, A. B. Sachid, S. B. Desai, M. Hettick, C. C. Hu, A. Javey, Field-effect transistors built from all two-dimensional material components. *ACS Nano* **8**, 6259–6264 (2014).
28. M. Yankowitz, J. Xue, D. Cormode, J. D. Sanchez-Yamagishi, K. Watanabe, T. Taniguchi, P. Jarillo-Herrero, P. Jacquod, B. J. LeRoy, Emergence of superlattice Dirac points in graphene on hexagonal boron nitride. *Nat. Phys.* **8**, 382–386 (2012).
29. W. Sheng, K. Luo, A. Zhou, Communication: Generalization of Koopmans' theorem to optical transitions in the Hubbard model of graphene nanodots. *J. Chem. Phys.* **142**, 021102 (2015).
30. H. M. Hill, A. F. Rigosi, A. Raja, A. Chernikov, C. Roquelet, T. F. Heinz, Exciton broadening in WS_2/graphene heterostructures. *Phys. Rev. B* **96**, 205401 (2017).
31. S. Gao, L. Yang, Renormalization of the quasiparticle band gap in doped two-dimensional materials from many-body calculations. *Phys. Rev. B* **96**, 155410 (2017).
32. Y. Liang, L. Yang, Carrier plasmon induced nonlinear band gap renormalization in two-dimensional semiconductors. *Phys. Rev. Lett.* **114**, 063001 (2015).
33. Y. Zhang, V. W. Brar, F. Wang, C. Girit, Y. Yayon, M. Panlasigui, A. Zettl, M. F. Crommie, Giant phonon-induced conductance in scanning tunnelling spectroscopy of gate-tunable graphene. *Nat. Phys.* **4**, 627–630 (2008).
34. Z. R. Kudrynskyi, M. A. Bhuiyan, O. Makarovsky, J. D. G. Greener, E. E. Vdovin, Z. D. Kovalyuk, Y. Cao, A. Mishchenko, K. S. Novoselov, P. H. Beton, L. Eaves, A. Patanè, Giant quantum hall plateau in graphene coupled to an InSe van der Waals crystal. *Phys. Rev. Lett.* **119**, 157701 (2017).

35. H. S. Jung, H.-Z. Tsai, D. Wong, C. Germany, S. Kahn, Y. Kim, A. S. Aikawa, D. K. Desai, G. F. Rodgers, A. J. Bradley, J. Velasco Jr., K. Watanabe, T. Taniguchi, F. Wang, A. Zettl, M. F. Crommie, Fabrication of gate-tunable graphene devices for scanning tunneling microscopy studies with Coulomb impurities. *J. Vis. Exp.* **2015**, e52711 (2015).
36. A. Castellanos-Gomez, M. Buscema, R. Molenaar, V. Singh, L. Janssen, H. S. van der Zant, G. A. Steele, Deterministic transfer of two-dimensional materials by all-dry viscoelastic stamping. *2D Mater.* **1**, 011002 (2014).
37. J. P. Perdew, K. Burke, M. Ernzerhof, Generalized gradient approximation made simple. *Phys. Rev. Lett.* **77**, 3865–3868 (1996).
38. P. Giannozzi, S. Baroni, N. Bonini, M. Calandra, R. Car, C. Cavazzoni, D. Ceresoli, G. L. Chiarotti, M. Cococcioni, I. Dabo, A. D. Corso, S. de Gironcoli, S. Fabris, G. Fratesi, R. Gebauer, U. Gerstmann, C. Gougoussis, A. Kokalj, M. Lazzeri, L. Martin-Samos, N. Marzari, F. Mauri, R. Mazzarello, S. Paolini, A. Pasquarello, L. Paulatto, C. Sbraccia, S. Scandolo, G. Sclauzero, A. P. Seitsonen, A. Smogunov, P. Umari, R. M. Wentzcovitch, QUANTUM ESPRESSO: A modular and open-source software project for quantum simulations of materials. *J. Phys. Condens. Matter* **21**, 395502 (2009).
39. H.-X. Zhong, S. Gao, J.-J. Shi, L. Yang, Quasiparticle band gaps, excitonic effects, and anisotropic optical properties of the monolayer distorted 1*T* diamond-chain structures ReS_2 and $ReSe_2$. *Phys. Rev. B* **92**, 115438 (2015).
40. M. Trushin, M. O. Goerbig, W. Belzig, Model prediction of self-rotating excitons in two-dimensional transition-metal dichalcogenides. *Phys. Rev. Lett.* **120**, 187401 (2018).
41. R. Geick, C. H. Perry, G. Rupprecht, Normal modes in hexagonal boron nitride. *Phys. Rev.* **146**, 543–547 (1966).
42. A. Laturia, M. L. Van de Put, W. G. Vandenberghe, Dielectric properties of hexagonal boron nitride and transition metal dichalcogenides: From monolayer to bulk. *npj 2D Mater. Appl.* **2**, 6 (2018).
43. P. Cudazzo, I. V. Tokatly, A. Rubio, Dielectric screening in two-dimensional insulators: Implications for excitonic and impurity states in graphane. *Phys. Rev. B* **84**, 085406 (2011).
44. T. C. Berkelbach, M. S. Hybertsen, D. R. Reichman, Theory of neutral and charged excitons in monolayer transition metal dichalcogenides. *Phys. Rev. B* **88**, 045318 (2013).
45. J. P. Echeverry, I. C. Gerber, Theoretical investigations of the anisotropic optical properties of distorted 1*T* ReS_2 and $ReSe_2$ monolayers, bilayers, and in the bulk limit. *Phys. Rev. B* **97**, 075123 (2018).
46. W. Tang, E. Sanville, G. Henkelman, A grid-based Bader analysis algorithm without lattice bias. *J. Phys. Condens. Matter* **21**, 084204 (2009).

Acknowledgments: We acknowledge the valuable discussion with J. Martin and K. Novoselov. **Funding:** J. Lu acknowledges the support from Ministry of Education (MOE) Tier 2 grants (R-143-000-682-112 and R-143-000-A06-112). M.Tr. is supported by the Director's Senior Research Fellowship from CA2DM at NUS (NRF Medium Sized Centre Programme R-723-000-001-281). S.A. acknowledges support from the Singapore MOE AcRF Tier 2 (MOE2017-T2-2-140) and the National University of Singapore Young Investigator Award (R-607-000-094-133). S.G. and L.Y. are supported by the NSF CAREER grant no. DMR-1455346 and the Air Force Office of Scientific Research grant no. FA9550-17-1-0304. The computational resources were provided by the Stampede of Teragrid at the Texas Advanced Computing Center through XSEDE. A.H.C.N. acknowledges the support from National Research Foundation of Singapore under its Medium-Sized Centre Programme. G.E. acknowledges the support from the MOE, Singapore, under AcRF Tier 2 (MOE2015-T2-2-123 and MOE2017-T2-1-134) and AcRF Tier 1 (R-144-000-387-114.). **Author contributions:** J. Lu supervised projects. Z.Q. performed STM measurements and data analysis with the help of H.F. H.F. performed atomic force microscopy measurements. M.Tr. devised the model with contributions from A.H.C.N. and S.A. E.L. performed the geometrical analysis of the moiré pattern under the supervision of S.A. I.V. performed photoluminescence measurements and data analysis with the help of H.F. under the supervision of G.E. S.G. performed the density functional theory calculation under the supervision of L.Y. M.Y. performed the calculation for estimating charge transfer at $ReSe_2$/G interface. K.W. and T.T. grew the h-BN for device. P.L., J. Li, and Z.Q. fabricated the device. J.S. and M.Te. helped with the STM measurements. J. Lu and Z.Q. prepared the manuscript with the contribution from M.Tr., I.V., G.E., S.G., L.Y., E.L., and J.W. All authors contributed to the scientific discussion and helped in writing the manuscript. **Competing interests:** The authors declare that they have no competing interests. **Data and materials availability:** All data needed to evaluate the conclusions in the paper are present in the paper and/or the Supplementary Materials. Additional data related to this paper may be requested from the authors.

Submitted 30 November 2018
Accepted 14 June 2019
Published 19 July 2019
10.1126/sciadv.aaw2347

Citation: Z. Qiu, M. Trushin, H. Fang, I. Verzhbitskiy, S. Gao, E. Laksono, M. Yang, P. Lyu, J. Li, J. Su, M. Telychko, K. Watanabe, T. Taniguchi, J. Wu, A. H. C. Neto, L. Yang, G. Eda, S. Adam, J. Lu, Giant gate-tunable bandgap renormalization and excitonic effects in a 2D semiconductor. *Sci. Adv.* **5**, eaaw2347 (2019).

Science Advances

Giant gate-tunable bandgap renormalization and excitonic effects in a 2D semiconductor

Zhizhan Qiu, Maxim Trushin, Hanyan Fang, Ivan Verzhbitskiy, Shiyuan Gao, Evan Laksono, Ming Yang, Pin Lyu, Jing Li, Jie Su, Mykola Telychko, Kenji Watanabe, Takashi Taniguchi, Jishan Wu, A. H. Castro Neto, Li Yang, Goki Eda, Shaffique Adam and Jiong Lu

Sci Adv **5** (7), eaaw2347.
DOI: 10.1126/sciadv.aaw2347